Applied Catalysis B: Environmental 287 (2021) 119982

Contents lists available at ScienceDirect

Applied Catalysis B: Environmental

journal homepage: www.elsevier.com/locate/apcatb

# Construction of $Fe_2O_3$ loaded and mesopore confined thin-layer titania catalyst for efficient $NH_3$-SCR of NO*x* with enhanced $H_2O/SO_2$ tolerance

Kai Guo [a,b,1], Ji Jiawei[a,1], Ryota Osuga [b], Yuxiang Zhu [a], Jingfang Sun [c], Changjin Tang [a,c,e,*], Junko N. Kondo [b,**], Lin Dong [a,c,d]

[a] School of Chemistry and Chemical Engineering, Nanjing University, Nanjing, China
[b] Institute of Innovation Research, Tokyo Institute of Technology, Yokohama, Japan
[c] Key Laboratory of Vehicles Emission Control of Jiangsu Province, Center of Modern Analysis, Nanjing University, Nanjing, China
[d] School of Environment, Nanjing University, Nanjing, China
[e] School of Environment, Nanjing Normal University, Nanjing, China

ARTICLE INFO

*Keywords:*
Thin-Layered titania
Mesoporous silica confined structure
Iron oxide loading
$NH_3$-SCR
sulfur resistance

ABSTRACT

$TiO_2$ is a famous support for selective catalytic reduction of NO with $NH_3$ ($NH_3$-SCR). Engineering the morphology and structure of $TiO_2$ is effective to modulate the interaction with surface dispersed component, providing further opportunity to improve catalytic performance. In this study, we rationally construct thin-layered titania confined in mesoporous silica *via* a surface grafting strategy. It exhibits high specific surface area with amorphous structure along mesopore channel, and much more Brønsted acid sites are generated than bulk $TiO_2$ due to defect induced oxygen-related species. After iron oxide loading, both the denitration activity and $H_2O/SO_2$ tolerance are greatly promoted as compared to conventional $Fe/TiO_2$. Further characterizations reveal the obtained catalyst displays uniform iron oxide dispersion and intense Fe-Ti interaction, resulting in superior redox behavior and increased acidity. Notably, it is found the introduction of $H_2O$ exhibits a promotional effect on NO conversion efficiency, which can be ascribed to enhancement of $NH_3$ adsorption capability. Besides, $SO_2$ has negligible disturbance on $NO/NH_3$ adsorption, leading to superior sulfur tolerance. The result of present study demonstrates vital role of surface structure engineering of $TiO_2$ for sustainable denitration, which opens up a new avenue for designing well-performed and stable $NH_3$-SCR catalysts.

## 1. Introduction

Nitrogen oxides (NO*x*), prominently emitted from the combustion of fossil fuel, is one major kind of atmospheric contaminants, and has caused serious environmental issues like photochemical smog, acid rain and greenhouse effect [1,2]. Therefore, the control of NO*x* has been increasingly concerned and under urgent demands. Among the diverse technologies developed to reduce NO*x*, selective catalytic reduction by $NH_3$ ($NH_3$-SCR) is accepted as the most effective one [3]. Currently, the vanadia-based catalysts, usually modified by $WO_3$ or $MoO_3$ on $TiO_2$, are commercially used as $NH_3$-SCR catalysts for the denitration of emission from stationary sources like power plant, industrial boiler, steel mill and process heater [4,5]. However, some weaknesses are shown by this catalyst system, such as narrow operation window (300−400 °C) and low $N_2$ selectivity at high temperature. Moreover, the high toxicity of vanadia to biological system make the dispose of waste catalysts a tough issue. Therefore, substantial attentions have been paid to develop environment-friendly $NH_3$-SCR catalysts operated at low temperatures for stationary sources.

Transition metal oxides like FeO *x* [6,7], MnO*x* [8,9], CuO [10,11], $CeO_2$ [12,13] and $Sm_2O_3$ [14,15] are tested as promising substitution for vanadium-based catalyst. Among them, iron oxide is a good choice due to their excellent redox ability of $Fe^{3+}/Fe^{2+}$ cycle and admirable $SO_2$-resistant property. On the other hand, as a typical material with sufficient surface acidity, $TiO_2$ has been extensively employed as support in both commercial and novel developed catalysts. It was found the structure and/or morphology of $TiO_2$ can have significant influence on its surface properties [16–18]. As well, the nature of surface active

* Corresponding author at: School of Chemistry and Chemical Engineering, Nanjing University, Nanjing, China.
** Corresponding author at: Institute of Innovation Research, Tokyo Institute of Technology, Yokohama, Japan.
*E-mail addresses:* tangcj@njnu.edu.cn (C. Tang), jnomura@res.titech.ac.jp (J.N. Kondo).
[1] These authors contribute equally to this work.

https://doi.org/10.1016/j.apcatb.2021.119982
Received 10 November 2020; Received in revised form 10 January 2021; Accepted 5 February 2021
Available online 13 February 2021

components can also be effectively tuned, which dictates the final catalytic performance. He et al. [19] synthesized VWTi catalysts with two different methods and obvious difference was exhibited. The catalyst fabricated by co-precipitation revealed small and poorly ordered $TiO_2$ particles. As a result, new O = $VO_3$ and O = $WO_4$ sites were formed with abundant defects and increased ammonia adsorption capacity were obtained. Smirniotis et al. [20,21] developed a novel catalyst with metal oxides confined in titania nanotubes (TNT) for $NH_3$-SCR reaction. The surface structure and tubular morphology of TNT were claimed to be responsible for promoted NO conversion. These results collectively indicate controlling of $TiO_2$ surface structure could be an effective way to improve its catalytic performance in $NH_3$-SCR.

In addition to activity improvement, good water and sulfur tolerance is also required for developing durable $NH_3$-SCR catalysts. Water is usually an unavoidable component in flue gas from stationary sources, since it comes from the combustion of fossil fuel. In previous studies [22–24], it is widely observed that the introduction of water into $NH_3$-SCR reaction system could result in an apparent decrease of catalyst denitration performance at low temperatures, since the competition adsorption between $H_2O$ with $NH_3$ on catalyst surface interfered the successive reduction of NO. As for catalyst deactivation by $SO_2$, it generally consists of three steps: $SO_2$ adsorption, $SO_2$ oxidation and deposition of sulfates [25]. It is reasonable that weakened $SO_2$ adsorption is crucial to alleviate $SO_2$ poisoning. Kwon et al. [26] found that modification of $VOx/TiO_2$ catalyst with molybdenum could reduce $SO_2$ adsorption through suppressing the reaction of $SO_2$ with terminal V = O. As a result, improved sulfur resistance is obtained. Liu et al. [27] explored $TiO_2$-$SiO_2$ as a novel support for $NH_3$-SCR. It was found that after $SiO_2$ introduction, the Brønsted acid sites were enriched, which lead to inhibited $SO_2$ adsorption and reduced accumulation of sulfates. As such, the Ce/TiSi catalyst showed strong resistance to $SO_2$. Interestingly, it is found that apart from chemical modification, the change of textural structure could also have great impact on the working lifespan of $NH_3$-SCR catalyst under $SO_2$. Yu et al. [28] synthesized a novel $MnO_2$-$Fe_2O_3$-$CeO_2$-$TiO_2$ catalyst with enormous mesoporous structure for low-temperature $NH_3$-SCR. The catalyst sustained 60 h operation in $SO_2$-contianing atmosphere. Quantitative result showed that ammonium bisulfate (ABS), which was a dominant poisoning species at low temperatures, did not accumulated on catalyst surface with prolonged operation. As such, they inferred the presence of mesopores was helpful for ammonium bisulfate decomposition, possibly achieving a dynamic balance with ABS deposition. In our recent study, we found that by simply increasing support pore size, ABS decomposition could be effectively promoted, resulting in excellent $SO_2$ resistant catalyst [29]. Under the inspiration of these previous efforts, we try to integrate the two aspects, surface modulation and mesoporous structure engineering into one catalyst system. That is, coating thin-layered titania in mesoporous silica as an efficient support. To the best of our knowledge, this represents the first study to employ mesoporous silica confined $TiO_2$ as a novel support for $NH_3$-SCR. Iron oxide with good $SO_2$ resistance is subsequently loaded onto the as prepared thin-layered titania. The prepared catalyst is systematically characterized to disclose the key factors accounting for superior catalytic performance. As well, the role of this unique structure in improving sulfur tolerance is also explored. The results obtained in the present study may enlighten the development of novel catalyst with excellent activity and superior $SO_2/H_2O$ tolerance for sustainable denitration.

## 2. Experiments

### 2.1. Catalyst preparation

Mesoporous silica SBA-15 was synthesized according to the previous literature [30]. In a typical synthesis, Pluronic P123 (5.0 g, Sigma-Aldrich Co., Ltd.) was used as soft template and dissolved in a solution containing 12 M HCl (17.02 g, Tokyo Chemical Industry Co., Ltd.) and deionized water (183 g) at 40 °C. Then, 10.5 g of Tetraethoxysilane (TEOS, Tokyo Chemical Industry Co., Ltd.) was added dropwise into the above solution. The mixture was stirred (40 °C, 24 h) and further aged (100 °C, 24 h). The obtained white solid was collected, washed by deionized water and ethanol (Wako Pure Chemical Industries, Ltd.) for several times and dried at 100 °C overnight. The template was then removed by calcination at 550 °C for 5 h.

To realize thin-layered titania coating on mesoporous silica, the procedure is as follows. After evacuation treatment (200 °C, 2 h) to remove surface adsorbed water, 2.0 g SBA-15 was immersed in super dehydrated toluene (50 mL, Wako Pure Chemical Industries, Ltd.) with $Ti(OC_3H_7)_4$ (Kojundo Chemical Laboratory Co., Ltd.) dissolved. The Ti/Si ratio is set as 0.088, which has been confirmed as the saturation feed amount for one time coating of Ti precursor, the experiment data is shown in **Figure S1**. The mixture was refluxed at 120 °C under Ar atmosphere for 3 h. The solid was collected by filtration, washed with hexane to remove the unreacted precursor. After drying at 100 °C, the sample was calcined at 450 °C for 4 h to solidify Ti-O-Ti network. The obtained sample was denoted as Ti@Si-1. The above procedure was repeated for 2 and 3 times to extend the coverage of titania layer on SBA-15, and the corresponding samples were labeled as Ti@Si-2 and Ti@Si-3, respectively.

The introduction of iron oxide on mesoporous silica confined titania was performed by a wetness impregnation method. Calculated Fe $(NO_3)_3{\cdot}9H_2O$ (20 wt% in terms of $Fe_2O_3$, Wako Pure Chemical Industries, Ltd.) was dissolved in 30 ml deionized water with 0.5 g Ti@Si added. The suspension was vigorously stirred for 2 h and excess water was evaporated at 80 °C under oil bath. The collected sample was further dried at 100 °C overnight. Finally, the catalyst was obtained by calcination at 450 °C for 4 h in muffle furnace and labeled as Fe/Ti@Si. As comparison, the catalyst by impregnating $Fe(NO_3)_3{\cdot}9H_2O$ on commercial $TiO_2$ was prepared and denoted as $Fe/TiO_2$.

### 2.2. Catalytic performance and poisoning resistance evaluation

$NH_3$-SCR performance of the prepared catalysts was evaluated in fixed-bed quartz reactor (8 mm internal diameter) under atmospheric pressure. The feed gas contained 500 ppm NO, 500 ppm $NH_3$, 5% $O_2$, and Ar in balance. The total flow rate was kept as 200 mL/min (the weight hourly space velocity, WHSV, was calculated to be 75,000 mL $g^{-1}$ $h^{-1}$). Before activity test, the catalyst was pretreated in purified Ar stream at 200 °C for 1 h to remove surface impurity. Then the feed gas was switched on, and the catalytic activity data were collected at every target temperature after stabilizing for 30 min. When considering water effect, the reaction proceeded in same manner with 5% vol $H_2O$ involved in feed gas using a heated bubbler. In addition, the sulfur and water resistance test of catalyst was carried out as followed procedure. The $NH_3$-SCR reaction was performed by holding the reaction temperature at 225 °C to achieve reaction steady state. Then $SO_2$ (200 ppm) and water vapor (5 vol%)was subsequently introduced into the system. The concentration of effluent gas was continuously analyzed by an IS10 FT-IR spectrometer. The NO conversion and $N_2$ selectivity was calculated according to the following equations:

$$NO\ \text{conversion}(\%) = \frac{[NO]_{in} - [NO]_{out}}{[NO]_{in}} \times 100\% \quad (1)$$

$$N_2\ \text{selectivity}(\%) = \frac{[NO]_{in} - [NO]_{out} + [NH_3]_{in} - [NH_3]_{out} - [NO_2]_{out} - 2[N_2O]_{out}}{[NO]_{in} - [NO]_{out} + [NH_3]_{in} - [NH_3]_{out}} \times 100\% \quad (2)$$

### 2.3. Characterizations

The BET surface area, total pore volume and average pore diameter were determined by $N_2$ adsorption-desorption isotherms at -196 °C

using Belsorp Mini, BEL Japan. Powder X-ray diffraction (XRD) patterns were recorded on a Rigaku Ultima III using a Cu Kα radiation source. The intensity data were collected at 2θ range from 10 to 80°. The X-ray tube was operated at 40kV and 40 mA. Transmission electron microscopy (TEM) images were acquired on a JEM-2100 instrument at an acceleration voltage of 200 kV. Elemental analysis was performed on an inductively plasma-atomic emission spectrometer (ICP-AES, Shimadzu ICPE-9000 spectrometer). X-ray photoelectron spectroscopy (XPS) measurements were conducted on a PHI 5000 Versa Probe system with a monochromatic Al Kα radiation (1486.6 eV, 15kW). All binding energies were calibrated with the adventitious C 1s (284.6 eV). Fourier transform infrared (FT-IR) spectra were recorded using JASCO 4100 FT-IR spectrometer equipped with a mercury cadmium telluride (MCT) detector at a resolution of 4 $cm^{-1}$ with 64 scans. The sample was pressed into a self-supporting disk (20 nm diameter), and placed in center of IR cell to realize the evacuation and adsorption. Diffuse reflectance ultraviolet-visible light (DR-UV–vis) absorption spectra were measured with a JASCO V-650 spectrophotometer and converted into the absorption spectra using the Kubelka-Munk function. Ammonia temperature-programmed desorption ($NH_3$-TPD) profiles were collected on a BEL-CAT (MicrotracBEL) instrument. The samples were pre-saturated with $NH_3$ and then flushed with He to remove physisorbed $NH_3$. The desorption patterns were obtained by increasing the temperature from 100 °C to 600 °C at rate of 5 °C/min. Hydrogen temperature-programmed reduction tests were carried out with BELCAT II (MicrotracBEL). The samples were pretreated at 200 °C for 2 h in Ar flow before the experiments. Then the TPR profiles were collected by passing 5% $H_2$/Ar from room temperature to 900 °C at rate of 5 °C/min. *In situ* diffuse reflection Fourier transform infrared (DRIFT) experiments were performed on a Nicolet Nexus 5700 FT-IR spectrometer equipped with a MCT detector at a resolution of 4 $cm^{-1}$ averaging 32 scans, and a diffuse reflectance reaction cell (HARRICK) with KBr window was used. The sample was pretreated at 450 °C for 1 h with $N_2$ flow to eliminate surface contaminants, then the background was collected at various target temperatures during the cooling process.

## 3. Results and discussion

### 3.1. Structure and chemical properties of thin-layered titania confined in SBA-15

Mesoporous silica SBA-15 is considered as a suitable substrate to obtain thin-layered titania. During Ti@Si preparation, the $Ti(OC_3H_7)_4$ precursor could react with surface hydroxyl groups (−OH) on SBA-15 (Fig. 1a). As shown by the dash line in Fig. 1b, typical C–H stretching vibrations at 2800−3000 $cm^{-1}$ are clearly observed, implying successful anchoring of Ti precursor on SBA-15. Meanwhile, the signal of surface silanol at 3744 $cm^{-1}$ almost disappears, suggesting Ti grafting is accomplished at the expense of silanol consumption. It is obvious under calcination, the −CH groups are removed. Simultaneously, a small part of Si−OH is recovered, which is probably induced by the reaction of water in air with surface Si-O-Si. Based on the fact that some isolated silanol groups are still present, SBA-15 surface is not considered to be fully covered by $TiO_2$. It is previously reported that for amorphous silica that was completely evacuated, the concentration of Si and OH on the surface are 2.80 and 1.55 $nm^{-2}$[31]. We have also measured the density of OH groups on SBA-15 by IR method and the value gives 1.5 $nm^{-2}$ [32]. Based on the measured surface area of SBA-15 (812 $m^2$/g, Table 1), the ratios of $Si_{(surface)}/Si_{(total)}$ and $OH/Si_{(total)}$ are deduced to be 0.23 and 0.12, respectively. By considering the actual Ti/Si ratio in Ti@Si-1

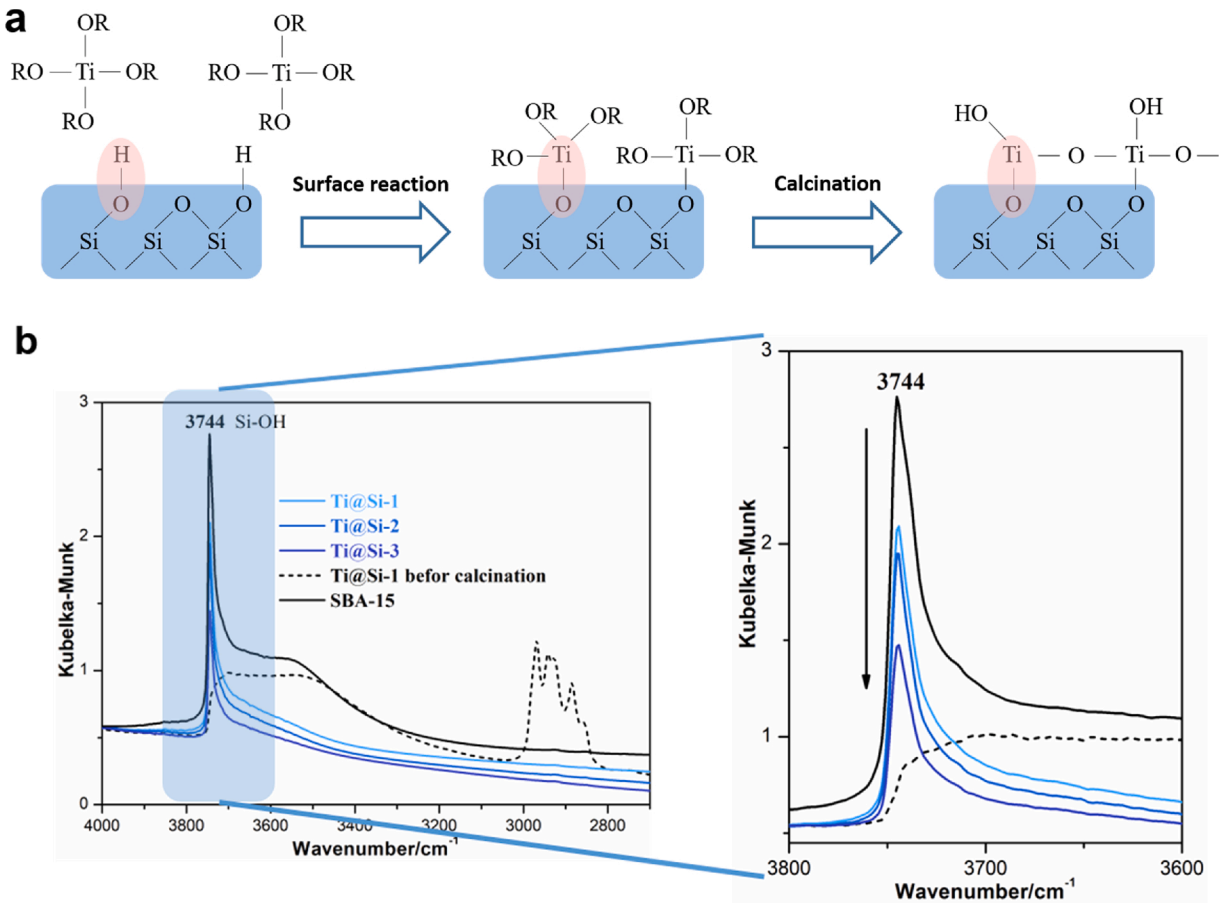


**Fig. 1.** (a) Schematic illustration of the process of Ti grafting on SBA-15. (b) FT-IR spectra of Ti@Si samples and SBA-15. The spectra were recorded at room temperature after evacuation at 150 °C for 1 h.

**Table 1**
The basic properties of Ti@Si samples.

| | Ti/Si ratio | | $TiO_2$ wt% | $S_{BET}$ /$m^2$ $g^{-1}$ | Pore size/nm | Total pore volume/$cm^3$ $g^{-1}$ | Micropore volume/$cm^3$ $g^{-1}$ |
|---|---|---|---|---|---|---|---|
| | Nominal | Actual | | | | | |
| SBA-15 | – | – | – | 812 | 8.3 | 1.45 | 0.15 |
| Ti@Si-1 | 0.088 | 0.075 | 9.97 | 724 | 8.1 | 1.08 | 0.08 |
| Ti@Si-2 | 0.176 | 0.142 | 18.67 | 665 | 8.0 | 1.01 | 0.06 |
| Ti@Si-3 | 0.264 | 0.172 | 22.86 | 583 | 7.8 | 0.95 | 0.03 |

(0.075, Table 1), we can easily calculate the Ti/OH on Ti@Si-1 to be 0.62, indicating the first coating process roughly covers 62% surface of SBA-15. In order to increase the coverage, the loading is repeated. From Fig. 1b, we can see the Si−OH signal is dramatically reduced with repeated $TiO_2$ loading, indicating the successive grafting of $TiO_2$ layer on SBA-15. The detailed $TiO_2$ loading determined from ICP measurement is listed in Table 1.

To examine structural changes after $TiO_2$ coating on SBA-15, the nitrogen adsorption-desorption isotherms of Ti@Si and SBA-15 are recorded (Fig. 2a). It is found all isotherms exhibit a comparable H1 type hysteresis loop, suggesting negligible disturbance of mesopores. This is also supported by small angle XRD result (Fig. 2b). However, the total volume is decreased with repeated titania loading. The results suggest $TiO_2$ is introduced into the pore channel of SBA-15 but does not induce obvious pore blocking. Thus, it is inferred the $TiO_2$ is confined in mesopore as thin-layered structure. Moreover, we can see from Table 1 that the pore size is slightly decreased from 8.3 nm to 7.8 nm after successive Ti coating, which can be well interpreted as the minorly increased thickness of $TiO_2$ layer. Notably, the micropore volume in SBA-15 exhibits a significant reduction, probably as a result of dense $TiO_2$ coating

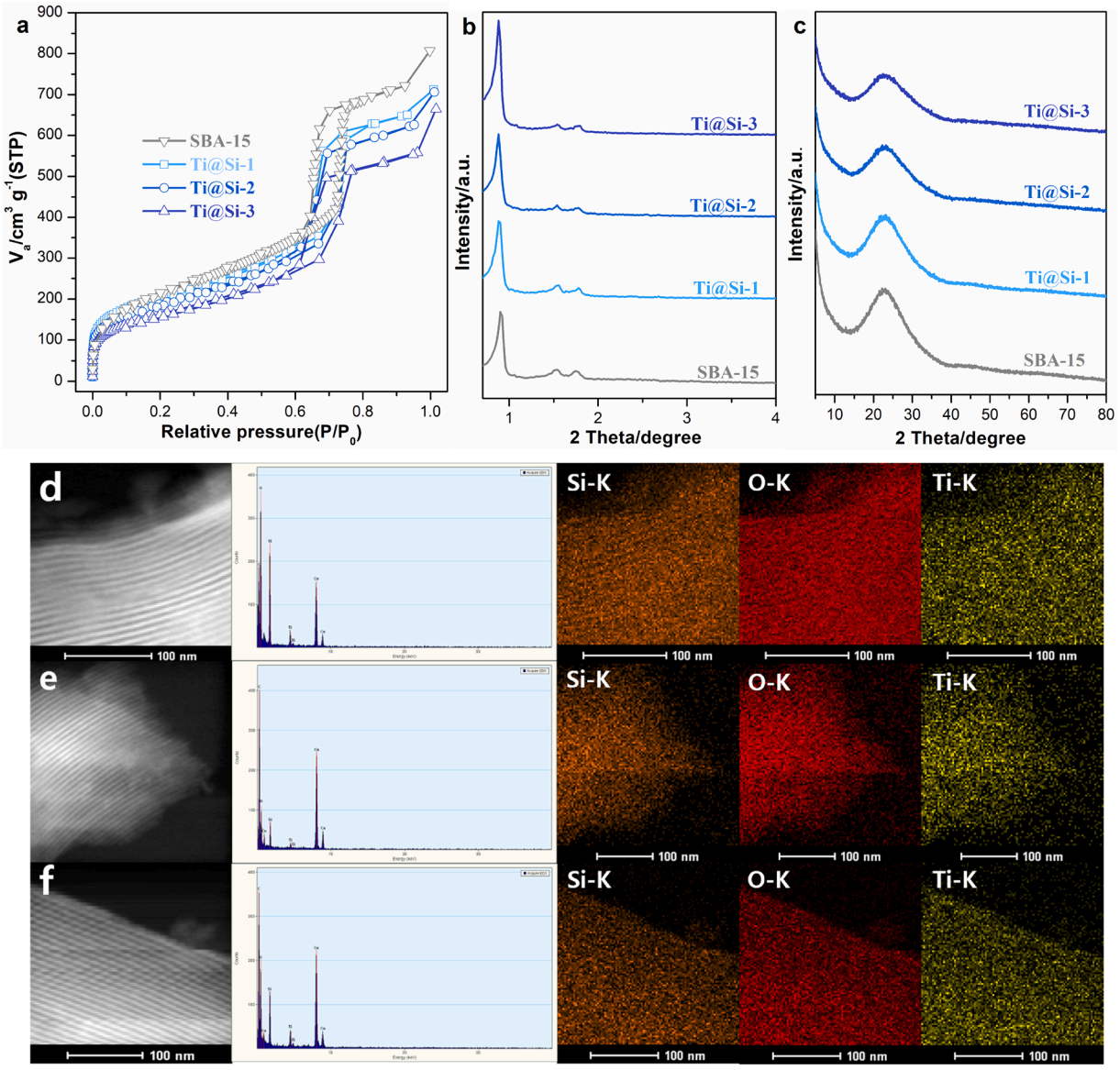


**Fig. 2.** (a) $N_2$ adsorption-desorption isotherms (b) small angle XRD and (c) XRD patterns of Ti@Si and SBA-15, HAADF-STEM and element mapping images of (d) Ti@Si-1 (e) Ti@Si-2 and (f) Ti@Si-3.

on SBA-15 surface. Since the micropores of SBA-15 is mainly originated from the removal of template (PEO branch in P123) penetrating into pore channel wall, the expansion of $TiO_2$ layer confined in mesopore would certainly decrease micropore volume. By examining the actual value of reduced micropore volume, we can roughly calculate the coverage of $TiO_2$ layer on SBA-15 for Ti@Si-3 sample approaches 75%.

To further explore the nature of surface Ti species, wide angle XRD characterization is operated and the result is depicted in Fig. 2**c**. No crystalline peak is found with increased $TiO_2$ coating except for a broad diffraction from SBA-15 skeleton. It confirms the $TiO_2$ layers are stabilized in amorphous state on SBA-15 even with the surface loading as high as 22.86 wt.%. This can be viewed as a solid evidence for the formation of strong Ti-O-Si and short ranged Ti-O-Ti bonds. Moreover, the HAADF-STEM images (Fig. 2**d, e, f**) confirms the preservation of ordered mesoporous structure and no $TiO_2$ particles are found (**Figure S2**). Since both $TiO_2$ layer and SBA-15 substrate are amorphous structure, no evident phase difference is revealed. However, EDS mapping analysis clearly shows the homogeneous distribution of Ti element on SBA-15. The result further confirms titania is introduced into the pore channel of SBA-15 as thin-layered structure, which is in line with results from $N_2$ adsorption-desorption and XRD characterizations.

Based on the information obtained above, a brief illustration of $TiO_2$ layers confined in SBA-15 with repeated treatment is shown in Scheme 1.It is considered that the first layer was formed at a partial occupancy of SBA-15 surface, and the second treatment resulted in formation of new layer together with the supplement of the first layer. Similarly, with the assistance of the third treatment, not only the thickness but also the coverage of $TiO_2$ layer obviously increases, which can be reasonably deduced from the reductions of pore size and micropore volume of SBA-15.

Apart from geometrical structure, the electronic property is also studied. Fig. 3**a** shows the results of diffuse reflectance UV–vis spectra. The pattern of bulk $TiO_2$ is listed for comparison. It can be found the absorption bands of Ti@Si samples show prominent distinction with that of $TiO_2$. This shows the unique electron property exhibited by metal oxides with ultra-thin structure [33]. It is reported that for two dimension semiconductor material, the band gap depends highly on the size of strictly limited dimension [34]. In the case here, the shift of absorption edge of Ti@Si to higher wavelength with repeated treatment suggests the gradual growth of $TiO_2$ layer in thickness.

The oxidation state of Ti element is explored by XPS measurement. Fig. 3**b** compares the XPS spectra of Ti 2p in Ti@Si with that of bulk $TiO_2$. For bulk $TiO_2$ which exclusively contains Ti-O-Ti structure, the photoelectron peaks for Ti $2p_{1/2}$ and $2p_{3/2}$ are observed at around 464.5 and 458.7 eV, respectively. Nevertheless, the Ti $2p_{3/2}$ peak of Ti@Si-1 is found to shift to higher binding energy (459.8 eV). This change is rationally considered as the formation of amorphous titania structure on $SiO_2$, which owns abundant structural defects and production of plenty of Si-O-Ti bond [33]. The peak intensity of Ti 2p gradually increases with $TiO_2$ loading repeated, in line with the fact that more $TiO_2$ was anchored on the surface from Ti@Si-1 to Ti@Si-3. Meanwhile, it is observed that the binding energy of Ti 2p slightly deviated to that of bulk $TiO_2$, which explains the electronic state of accumulated titania layers has the tendency getting close to $TiO_2$ due to more Ti-O-Ti bond is formed in Ti@Si-2 and Ti@Si-3 with layers stacking. Combined the results of UV–vis and XPS, it could be confirmed that the electronic property of amorphous titania confined in SBA-15 shows much difference with that of bulk $TiO_2$, which is expected to have significant effect on the property of surface adsorption and the loaded active species.

Fig. 4**a** gives the $NH_3$-TPD result of Ti@Si and bulk $TiO_2$, the quantitative data of desorbed $NH_3$ are summarized in **Table S1**. In contrast to the minor signal observed for bulk $TiO_2$ with acid amount of only 0.1275 mmol/g, the $NH_3$ desorption curve of Ti@Si-1 exhibits significant enhancement and desorbed amount is promoted to 0.4990 mmol/g. With further extending of $TiO_2$ coverage, the $NH_3$ adsorption further increases for Ti@Si-2 as 0.5587 mmol/g and the highest amount of $NH_3$ adsorption is found for Ti@Si-3 with amount of calculated as 0.5796 mmol/g. The result of $NH_3$-TPD clearly show that construction of amorphous thin-layered $TiO_2$ in SBA-15 is conducive to enhance surface acid amount, which is beneficial to promote $NH_3$-SCR activity.

The nature of surface adsorption species is identified by *in situ* FT-IR, and results are shown in Fig. 4**b-4e**. It can be clearly found that after $NH_3$ adsorbed on bulk $TiO_2$ surface, IR bands at 1600 and 1155 $cm^{-1}$ due to $NH_3$ vibration on Lewis acid sites gradually emerge with increasing $NH_3$ pressure, while the peak at 1442 $cm^{-1}$ attributed to $NH_4^+$ on Brønsted acid site is quite inferior even after exposed to 2000 Pa $NH_3$, implying the bulk $TiO_2$ surface is dominated by Lewis acid sites. While for Ti@Si samples, except for the existence of a band at 1606 $m^{-1}$ representing $NH_3$ on Lewis acid sites, the band at 1451 $cm^{-1}$ (1456 $cm^{-1}$ for Ti@Si-2 and 1446 $cm^{-1}$ for Ti@Si-3) ascribed to $NH_4^+$ on Brønsted acid sites is also obvious. Simultaneously, the intense negative band in OH region at *ca.* 3750 $cm^{-1}$ clearly emerges when $NH_3$ is introduced to all Ti@Si samples, suggesting the involvement of surface OH species in $NH_3$ adsorption. Moreover, the proportion of Brønsted acid sites to Lewis acid sites on Ti@Si shows an evident increase (Fig. 4f). The result demonstrates that repeated coating enhances Brønsted acidity of thin-layered titania due to extended coverage. It is well acknowledged that Brønsted acid site on oxide surface is represented by acidic −OH group on metal atom, which could adsorb $NH_3$ molecule to M-O-$NH_4^+$. With that point in mind, we suppose that due to numerous structure defects on layered titania, much more adsorbed oxygen species like surface −OH groups can be obtained, which can be also evidenced by O 1s XPS spectra of Ti@Si samples in **Figure S3**. As a consequence, significant Brønsted acid sites are generated. The speculation proposed here also finely agreed with the increased binding energies of Ti atoms in Ti@Si than $TiO_2$. Besides, the comparison of IR results from three Ti@Si samples show negligible difference in adsorption configuration, indicating the similar surface acid sites of amorphous thin-layered titania in SBA-15.

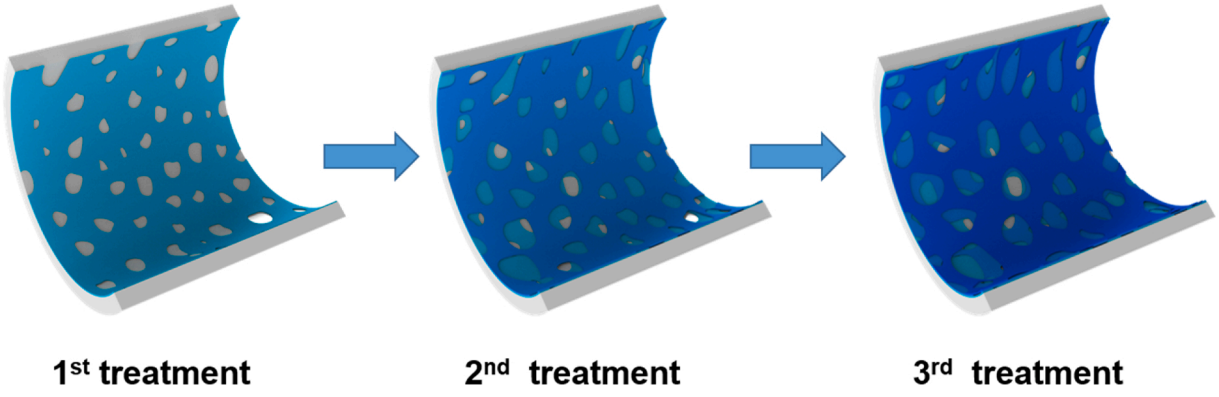


**Scheme 1.** Illustration of the formation of thin-layered titania on SBA-15 with repeated coating.

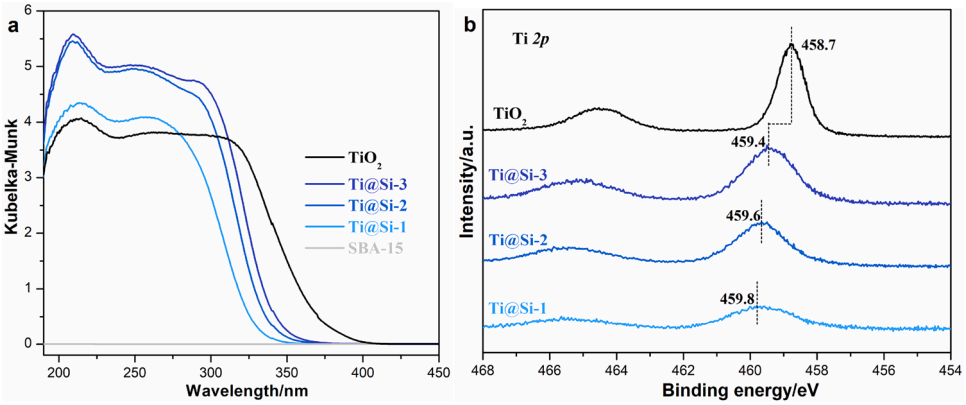


**Fig. 3.** (a) Diffuse reflectance UV–vis and (b) Ti 2p XPS spectra of the Ti@Si.

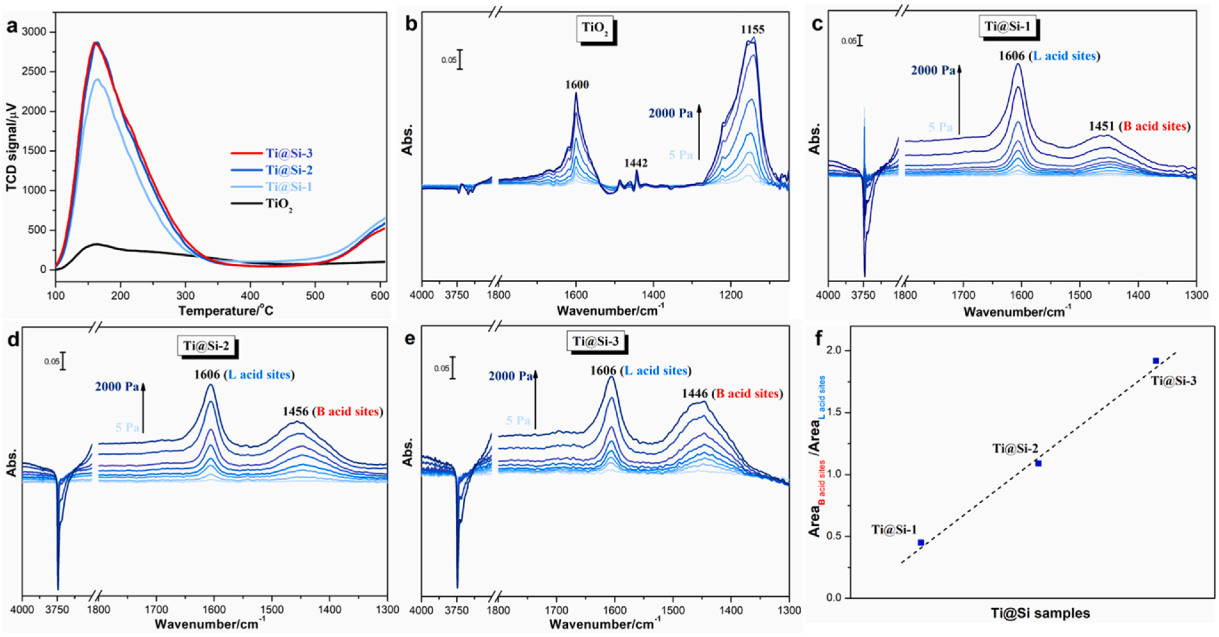


**Fig. 4.** (a) $NH_3$-TPD, (b-e) *in situ* FT-IR spectra of $NH_3$ adsorption on various samples and (f) IR peak area ratios (Brønsted acid sites/Lewis acid sites) of Ti@Si series.

### *3.2. $NH_3$-SCR and anti-poisoning performance of iron oxide supported thin-layered titania catalysts*

$TiO_2$ is widely used as an efficient support for $NH_3$-SCR reaction and $Fe/TiO_2$ is a notable catalyst. Hence, in the present study, iron oxide is chosen as an active component to deposit on Ti@Si for exploring the effect of support structure on $NH_3$-SCR performance. Fig. 5**a** displays the activity result. For the reference $Fe/TiO_2$ catalyst, it is found the NO conversion only acquires maximum value of 78% at 350 °C. Further temperature increment leads to activity declining, which could be ascribed to the over-oxidation of $NH_3$ to nitric oxides at high temperatures [35]. As for Fe/Ti@Si samples, the Fe/Ti@Si-1 shows much higher denitration efficiency in the temperature range of 200–400 °C. It suggests the spreading of thin-layered titania along the pore channel of SBA-15 provides abundant titania surface and anchoring sites for $Fe_2O_3$, which is advantageous to enhancement of catalytic performance. Moreover, repeated $TiO_2$ coating results in progressive elevation of catalytic activity in the whole temperature range. Apart from activity elevation, $N_2$ selectivity improvement is also obtained by Fe/Ti@Si catalysts, where Fig. 5**b** presents the data. It can be clearly seen that $N_2$ selectivity of $Fe/TiO_2$ obviously declines to only 84% at 400 °C, which is in consistence with its inferior performance due to $NH_3$ oxidation. While for Fe/Ti@Si catalysts, they display excellent $N_2$ selectivity (>96%) in entire test range, indicating the high efficiency in reducing NO by $NH_3$ to harmless $N_2$. The results can be further confirmed by $N_2O$ formation data in **Figure S4** and finely certify the superior $NH_3$-SCR performance of Fe/Ti@Si catalysts.

Due to the complex constituents in the real flue gas, the poisoning resistance of catalyst is quite important for practical application. As such, the impact of $H_2O$ on $NH_3$-SCR catalyst performance is accordingly explored. Fig. 5**c** presents the influence of 5 vol% $H_2O$ on the NO conversion of Fe/Ti@Si-3 catalyst. In our case, however, the existence of vapor surprisingly promotes the catalytic activity of Fe/Ti@Si-3 below 300 °C, which exhibits much different trend with the previous reports. $SO_2$ is another impurity that may deactivate $NH_3$-SCR catalyst. To further explore the impact of $SO_2$, the tolerance tests were carried out over Fe/Ti@Si-3 and $Fe/TiO_2$. After achieving steady state at 225 °C, $SO_2$ and vapor were stepwise introduced into the reaction system. As can be seen from Fig. 5d, the NO conversion of $Fe/TiO_2$ dramatically declined from 38% to 13% when 200 ppm $SO_2$ was injected. However, the introduction of 5% vapor did not show apparent influence. The result reveals that in comparison with water, the catalyst is more sensitive to sulfur oxide, which exerts an apparent negative effect on NO conversion. Remarkably, for Fe/Ti@Si catalyst, the NO conversion only

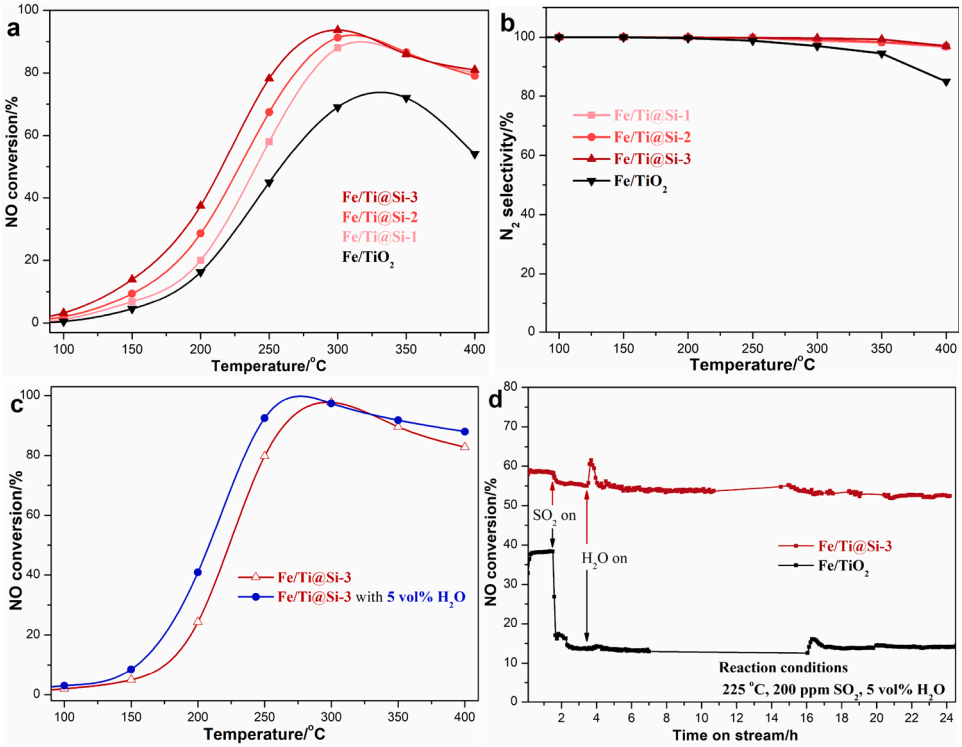


**Fig. 5.** (a) $NH_3$-SCR activities and (b) $N_2$ selectivity of Fe-based catalysts, (c) NO conversion of Fe/Ti@Si-3 in presence of water vapor, (d) Sulfur and water resistance tests of Fe/Ti@Si-3 and Fe/$TiO_2$. Reaction condition: 500 ppm $NH_3$, 500 ppm NO, 5% $O_2$, 200 ppm $SO_2$ and 5 vol% $H_2O$ (when used), WHSV: 75000 mL $g^{-1}$ $h^{-1}$.

slightly fluctuates (*ca.* 3%) when $SO_2$ was introduced, indicating minor inhibition effect is exhibited. Furthermore, the introduction of 5 vol% $H_2O$ also shows an instant promotion on the catalytic performance, but the effect seems not persistent in presence of $SO_2$. Thus, the distinct behaviors of the two catalysts working under simulated condition illustrates that Fe/Ti@Si catalyst with thin-layered titania encapsulated in mesoporous silica exhibits much superior resistance to $SO_2$ and $H_2O$, which is also better than generally reported commercial VWTi catalysts in the same condition [36,37].

### 3.3. *Insights into the improved deNOx efficiency and superior $H_2O/SO_2$ resistance*

To understand the reason for the distinct catalytic behaviors, the catalysts are further characterized. The $N_2$-sorption results are shown in **Figure S5** and Table 2. It could be seen that Fe/Ti@Si still maintained their ordered mesoporous structure as can be deduced from the preservation of H1 hysteresis loop in the isotherms. In comparison with pristine Ti@Si, the textural parameters show an obviously decrease due to encapsulation of Fe oxide in the mesopore channels. **Figure S6** shows the wide angle XRD patterns. For Fe/$TiO_2$ sample, in addition to the signal from $TiO_2$ support, X-ray diffractions attributed to α-$Fe_2O_3$ at $2\theta = 24.1°$, 33.2°, 35.6° and 54.1° are clearly observed. The peaks for iron oxide are also present in Fe/Ti@Si samples. However, they exhibit much poor intensity, suggesting the enhanced $Fe_2O_3$ dispersion. It is further confirmed by TEM and EDS mapping result. As can be seen from Fig. 6, tiny iron oxide particles are confined in the mesopore of Ti@Si support, while Fe/$TiO_2$ sample reveals the stacked bulk particles with size of *ca.*40−50 nm. EDS mapping images (**Figure S7**) also show the homogeneous distribution of Fe species along with surface Ti in Fe/Ti@Si, implying the close interaction between two components. It is believed that the highly available titania surface, mesopore confined environment and intense interface interaction are responsible for the improved dispersion of iron species.

**Table 2**
The textural property of various FeTi catalysts.

| | $S_{BET}$ ($m^2$ $g^{-1}$) | Pore volume ($cm^3$ $g^{-1}$) |
|---|---|---|
| Fe/$TiO_2$ | 57 | 0.41 |
| Fe/Ti@Si-1 | 487 | 0.93 |
| Fe/Ti@Si-2 | 467 | 0.87 |
| Fe/Ti@Si-3 | 442 | 0.75 |

To approach the electronic interaction between iron oxide and the supports, XPS characterization is carried out and the result is shown in Fig. 7. Comparing with pure support (Fig. 3b), it is found the binding energy of Ti 2p for Fe/$TiO_2$ and Fe/Ti@Si is red shifted. Moreover, the Ti 2p signals Fe/Ti@Si catalysts exhibit a much significant deviation. The phenomenon indicates that the thin-layered titania can withdraw more electrons from supported iron oxide than bulk $TiO_2$, implying the occurrence of strengthened Fe-O-Ti interface interaction. In the meantime, for Fe/Ti@Si samples, the Fe 2p signal is correspondingly induced to much higher value at 711.1 eV due to more electrons transferred to support. The prominent difference suggests the construction of thin-layered titania can significantly affect the electron density of supported iron oxide.

The redox property of catalysts is an important factor for $NH_3$-SCR. Fig. 8a shows the $H_2$-TPR profiles of these Fe-based catalysts. For Fe/$TiO_2$, a multiple reduction is exhibited, which can be ascribed to reduction of $Fe_2O_3$ to $Fe_3O_4$, $Fe_3O_4$ to FeO and FeO to metallic Fe. For Fe/Ti@Si, the process varies greatly. The reduction curve of Fe/Ti@Si-1 reveals a dominant $H_2$ consumption peak at 437.7 °C, which can be explained as synergistic reduction due to strong interfacial interaction between iron oxide and the thin-layered titania. Besides, the tiny peak emerges at 541.8 °C could be attributed to the reduction of minor iron oxide that is not directly contacted with titania layer. It is noted that with increase of titania coverage, the tiny peak gradually decreases and finally vanishes, which is in good agreement with the attribution of this peak to reduction from $Fe_2O_3$ particle on $SiO_2$. By comparing the reduction temperature with Fe/$TiO_2$, it is clear that the loading of iron

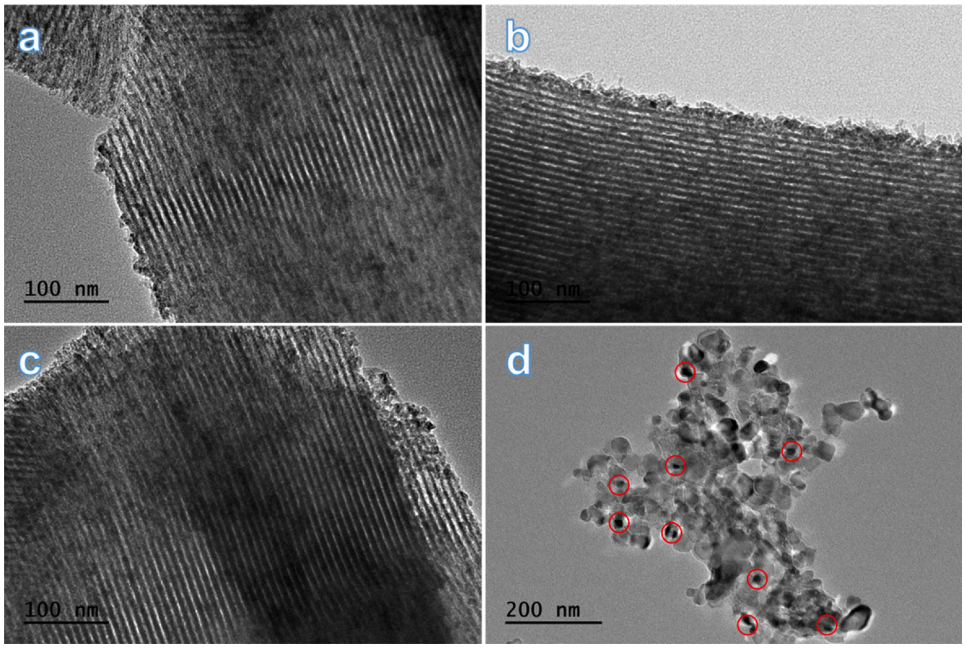


**Fig. 6.** TEM images of (a) Fe/Ti@Si-1, (b) Fe/Ti@Si-2, (c) Fe/Ti@Si-3 and (d) Fe/$TiO_2$.

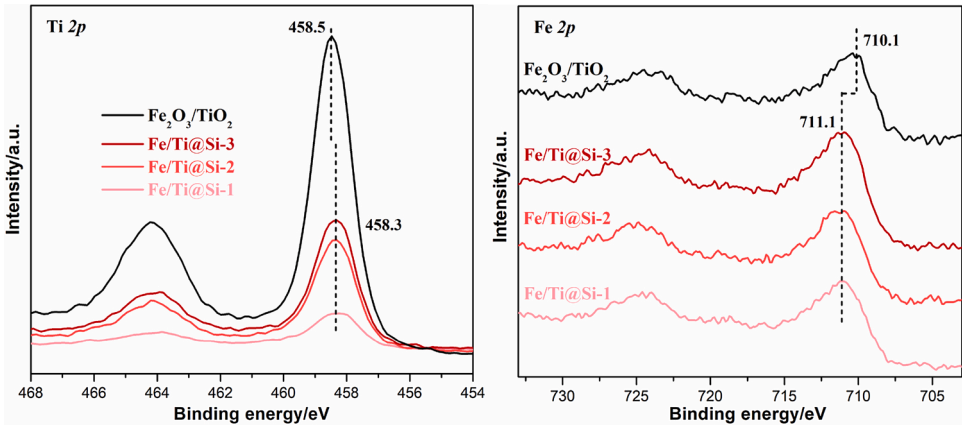


**Fig. 7.** Ti 2p and Fe 2p XPS spectra of FeTi catalysts.

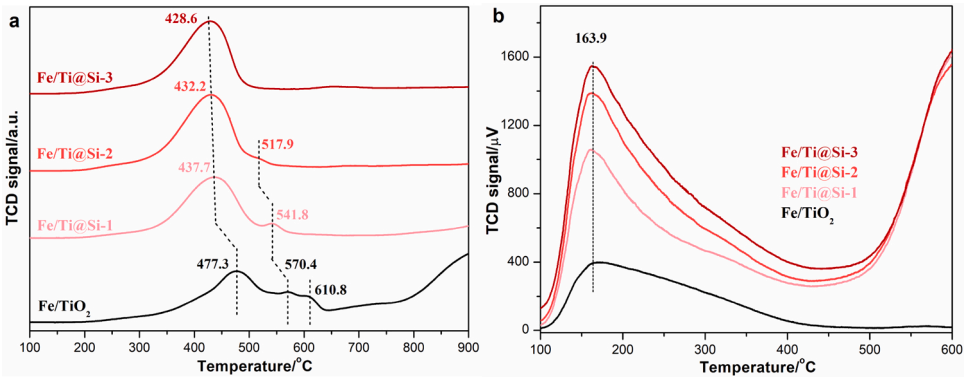


**Fig. 8.** (a) $H_2$-TPR and (b) $NH_3$-TPD curves of Fe/Ti@Si and Fe/$TiO_2$ catalysts.

oxide on thin-layered titania could prominently improve the redox property of catalysts.

The surface acidity of FeTi catalysts is characterized by $NH_3$-TPD and results are present in Fig. 8**b**. In all cases, the spectra show similar feature in 100−450 °C, with a broad peak centered at 163.9 °C. As compared with the $NH_3$-TPD curves of pure Ti@Si shownin Fig. 4a, the $NH_3$ desorption on weak acid sites (100−300 °C) is reduced. Nevertheless, the signal of $NH_3$ desorption from Fe/Ti@Si-1 is much higher

than $Fe/TiO_2$, suggesting the superior surface acidity of Fe/Ti@Si catalyst. In addition, dramatic $NH_3$ desorption above 500 °C for Fe/Ti@Si samples is observed while this signal is still absent for $Fe/TiO_2$. In contrast to Ti@Si, it is found the signal from high temperature desorption (corresponding to strong acid sites) is more obvious than that from low temperature (representing weak acid sites), suggesting great variation of surface acidity on Ti@Si *via* iron oxide modification. Moreover, the quantitative data of desorbed $NH_3$ in TPD of Fe based catalysts is shown in **Table S2**. The $NH_3$ adsorption amount on $Fe/TiO_2$ is 0.1263 mmol/g, while the data of iron oxide supported thin-layer titania sample, Fe/Ti@Si-1, shows significant enhancement to 0.4880 mmol/g. Furthermore, with repeating of titania coating on Ti@Si-1, the acid amount of Fe/Ti@Si-2 and Fe/Ti@Si-3 gradually elevates to 0.5539 and 0.6303 mmol/g, respectively. The result indicates that the employment of thin-layered titania as catalyst support can effectively promote the surface acid property of Fe-based catalyst, which conducive to obtain the high $NH_3$-SCR performance.

Figs. 9**a** and **9b** show the *in situ* DRIFT spectra of $NH_3$ adsorption on $Fe/TiO_2$ and Fe/Ti@Si-3, respectively. $Fe/TiO_2$ exhibits $NH_3$ adsorption signal at 1596 and 1187 $cm^{-1}$, attributing to $\delta_{as}$ and $\delta_s$ vibration modes of coordinated $NH_3$ species on Lewis acid sites [38]. An additional band at 1447 $cm^{-1}$ could be related to the vibration of $NH_4^+$ on Brønsted acid sites. As for Fe/Ti@Si-3, the bands at 1610 and 1454 $cm^{-1}$ ascribed to $NH_3$ on Lewis acid sites and $NH_4^+$ on Brønsted acid sites also appear. Moreover, another new band at 1579 $cm^{-1}$ which could be attributed to $–NH_2$ emerges [39]. It is believed that the adsorbed $NH_3$ species is activated *via* subtracting one hydrogen atom to $–NH_2$. The presence of this band confirms improved redox ability of Fe/Ti@Si-3 for promoted $NH_3$ activation, which conducive to subsequently NO reduction. It is noted that with temperature increasing, the adsorbed $NH_3$ species on $Fe/TiO_2$ totally desorbs at 400 °C, while there are still adsorbed species remained on Fe/Ti@Si-3 surface, demonstrating the higher thermal stability of adsorbed $NH_3$. The result is in well consistence with $NH_3$-TPD analysis.

To acquire the information regarding NO-related adsorbed species, the *in situ* DRIFTS of NO + $O_2$ adsorption are recorded and results are shown in Fig. 9**c** and **9d**. For $Fe/TiO_2$, the bands related to nitrate species in range of 1000−2000 $cm^{-1}$ emerge on the spectra after NO + $O_2$ adsorption. The detailed attributions could be related to bridged nitrate at 1625 $cm^{-1}$, chelating bidentate nitrate at 1582 and 1557 $cm^{-1}$, monodentate nitrate at 1496 and 1295 $cm^{-1}$ [40,41]. With temperature elevating from 50 °C to 300 °C, intensity of the peaks corresponding to bidentate and monodentate nitrate species gradually weaken while the bridged nitrate peak increases. The opposite evolution of peak intensity implies transformation of bidentate and monodentate nitrates to bridged nitrate species, of which the latter species is considered more stable at higher temperatures. Further elevating the temperature to 450 °C results in desorption of most nitrate species. As for Fe/Ti@Si-3, the exposure of NO + $O_2$ stream produces different nitro-related species. In addition to bridged nitrate at 1624 $cm^{-1}$ and chelating bidentate nitrate at 1578 $cm^{-1}$, the bands at 1676 $cm^{-1}$ and 1607 $cm^{-1}$ are identified as *cis*-$HNO_2$ and adsorbed $NO_2$, respectively. The generation of $NO_2$ over catalyst surface could effectively facilitate the reaction rate *via* "fast SCR" route, which can be viewed as an important factor for the superior catalytic performance of Fe/Ti@Si-3 catalyst.

Besides, we also try to disclose the inherent origin of impressive poisoning resistance of thin-layered titania catalyst, where a peculiar effect of vapor on catalyst performance has been observed in Fig. 5**b**. Since $H_2O$ mainly affects $NH_3$ adsorption [42,43], the origin of unique $H_2O$ promotion phenomenon is studied by $NH_3$ breakthrough experiments over Fe/Ti@Si-3. Briefly, the sample was firstly blowing by Ar at 200 °C for 1 h and temperature maintained in follow. Subsequently, 5 vol% $H_2O$ was introduced to sample for 30 min then switched off. After 10 min stabilizing, $NH_3$ was inlet to pass through the sample and effluent gas was analyzed by IR. The dry Ar pretreated sample was also proceeding with above procedure only without water vapor. It can be clearly seen in Fig. 10**a** that the $NH_3$ adsorption on Fe/Ti@Si-3 with dry Ar pretreatment becomes saturated in *ca.* 1100s. While for the sample pretreated with $H_2O$, the increasing trend of outlet $NH_3$ is much slower than dry Ar pretreated one, indicating more $NH_3$ molecules adsorb on catalyst surface. The quantitative evaluations of retained $NH_3$ on catalyst are calculated as 0.091 mmol/g and 0.134 mmol/g for both dry and

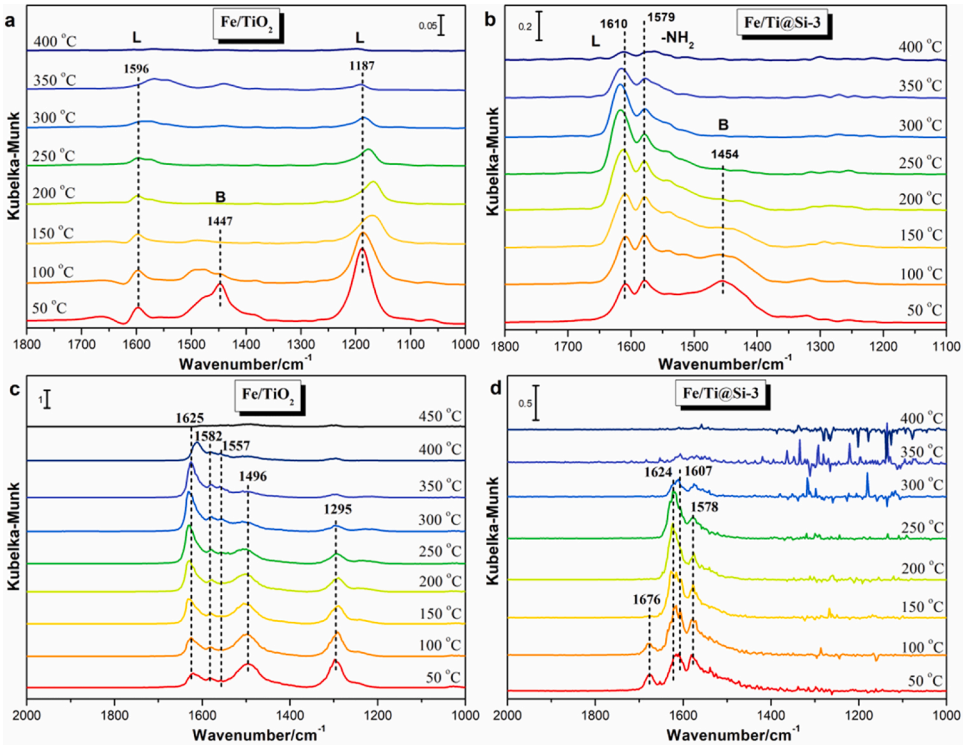


**Fig. 9.** *In situ* DRIFT spectra of $NH_3$ adsorbed on (a) $Fe/TiO_2$, (b) Fe/Ti@Si-3 and NO + $O_2$ adsorption on (c) $Fe/TiO_2$, (d) Fe/Ti@Si-3.

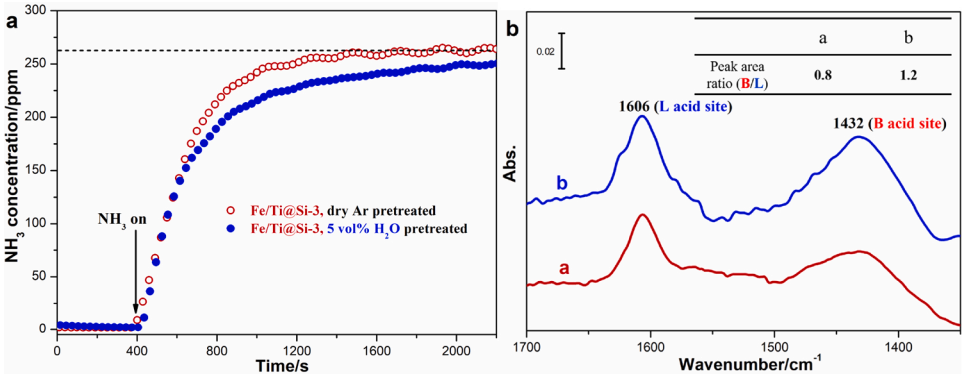


**Fig. 10.** (a) $NH_3$ breakthrough curve at 200 °C on Fe/Ti@Si-3 pretreated with dry Ar and 5 vol% $H_2O$/Ar, (b) *In situ* FT-IR spectra of $NH_3$ adsorption on Fe/Ti@Si-3 at 200 °C, a: without water pretreatment, b: with water pretreatment.

water pre-treated conditions. It can be rationally supposed that more acid sites are generated on Fe/Ti@Si-3 after $H_2O$ pretreatment. To further elucidate the inherent reason, the *in situ* FT-IR experiments of $NH_3$ adsorption with different pretreatment conditions are carried out, the results are shown in Fig. 10**b**. The spectrum **a** represents $NH_3$ adsorption on Fe/Ti@Si-3 at 200 °C without water pretreatment. It gives two IR bands at 1606 and 1432 $cm^{-1}$, ascribing to the vibration of $NH_3$ species on surface Lewis acid site (L) and Brønsted acid site (B), respectively. We integrate the peak area of two peaks and calculate peak area ratio of B to L as 0.8. In addition, Fe/Ti@Si-3 is also pretreated with $H_2O$ at 200 °C for 30 min, then $NH_3$ is allowed to adsorb on the sample to obtain spectrum **b**. It reveals similar peak attributions with the former spectrum. Nevertheless, the calculated peak area ratio (B/L) comes to 1.2, which is much higher than the result without $H_2O$ pretreatment. We have discussed previously that thin-layered titania is formed from the condensation of surface Ti-OR groups to defective oxide network (Ti-O-Ti) during calcination process. The distinct data clearly indicates the introduction of $H_2O$ to Fe/Ti@Si-3 surface can effectively promote the production of Brønsted acid sites, further suggests that $H_2O$ may dissociatively adsorb on Ti-O-Ti, leading to the generation of more surface Ti−OH[44,45], which acts like Brønsted acid sites for increased $NH_3$ adsorption. The result turns out the $H_2O$ pretreatment obviously increases the $NH_3$ adsorption capability, which certainly conducive to catalyst $NH_3$-SCR activity, instead of a poisoning factor.

It is known from Fig. 5**c** that Fe/Ti@Si-3 owns much better $SO_2$ resistance than Fe/$TiO_2$. To explore the possible reason, the competition adsorption of $SO_2$ with NO and $NH_3$ on different catalysts is operated and results are shown in Fig. 11. It can be seen from Fig. 11**a** that for Fe/$TiO_2$ catalyst, the IR bands at 1604, 1540 and 1456 $cm^{-1}$ resulting from $NH_3$ adsorption rapidly vanish with prolonged $SO_2$ exposure, while asymmetric vibration bands of O═S═O at 1319 and 1375 $cm^{-1}$ [46,47] due to $SO_2$ adsorption emerge and gradually intensify. Similarly, as can be seen from Fig. 11b, the pre-adsorbed nitrate species from NO + $O_2$ at 1606 and 1575 $cm^{-1}$ are replaced by asymmetric vibration bands of O═S═O at 1311, 1372 $cm^{-1}$ and water at 1625 $cm^{-1}$ [48] after $SO_2$ introduction. The variation of adsorbed species on catalyst surface

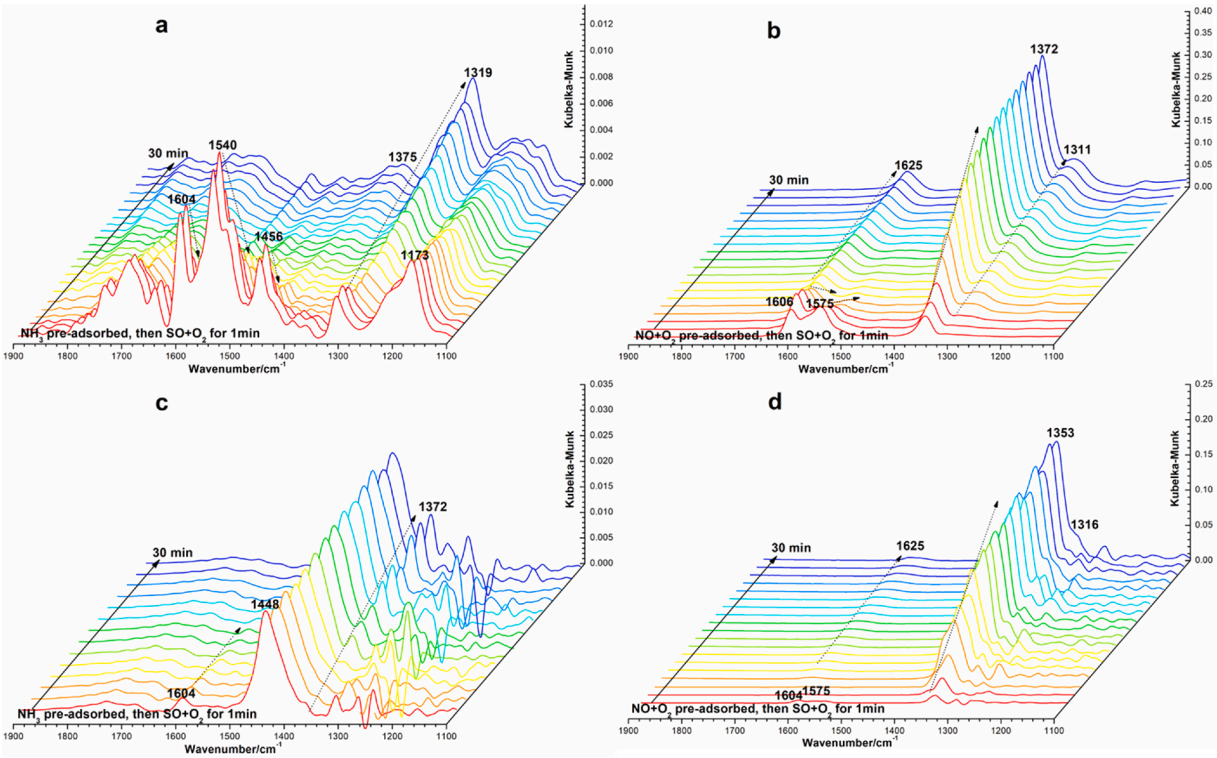


**Fig. 11.** *In situ* DRIFT spectra of $SO_2$+$O_2$ competing with pre-adsorbed $NH_3$ and NO + $O_2$ on Fe/$TiO_2$ (a, b) and Fe/Ti@Si-3 (c, d).

soundly demonstrates that the introduction of $SO_2$ could seriously interfere the stable adsorption of NO and $NH_3$ over Fe/$TiO_2$,thus cut off the successive NO reduction. Due to the dominant adsorption of $SO_2$, the $NH_3$-SCR performance of Fe/$TiO_2$ is significantly reduced. The same experiment is also conducted over Fe/Ti@Si-3 catalyst. After $NH_3$ adsorption, a minor peak at 1604 $cm^{-1}$ and major peak belongs to $NH_4^+$ on Brønsted acid sites at 1448 $cm^{-1}$ are detected. Following this step, $SO_2$ is injected into the cell and the spectra are depicted in Fig. 11**c**. Remarkably, the IR bands for $NH_3$ adsorption are hardly affected on catalyst surface while the bands of O═S═O vibration at 1372 $cm^{-1}$ slowly increases. As for $SO_2$ adsorption on pre-adsorbed NO + $O_2$, the signal from nitrate species at 1604 and 1575 $cm^{-1}$ gradually overlaps with water band at 1625 $cm^{-1}$, along with the development of adsorbed $SO_2$ at 1353 and 1316 $cm^{-1}$ [49,50]. It could be clearly observed that introducing $SO_2$ rarely obstructs the surface pre-adsorbed species. It is highly possible that the stable adsorption of $NH_3$ and NO related species in the presence of $SO_2$ ensures the reliable proceeding of $NH_3$-SCR reaction over Fe/Ti@Si-3. As such, the injection of $SO_2$ can barely deactivate the catalyst. Due to the fact that Fe/Ti@Si-3 reveals much improved surface acid property, it is speculated that the presence of abundant acid sites on thin-layered titania effectively resists the $SO_2$ adsorption, resulting in excellent $SO_2$ tolerance in $NH_3$-SCR reaction.

## 4. Conclusions

In summary, thin-layered titania confined in SBA-15 is successfully prepared *via* a grafting strategy, and iron oxide is subsequently loaded on the Ti@Si support to construct $NH_3$-SCR catalyst. Owing to abundant oxygen-derivatives adsorbed on the thin-layered titania with amorphous structure, significant Brønsted acid sites are generated. Moreover, the electronic state of Ti is prominently regulated. After Fe oxide loading, the catalysts exhibit excellent denitration efficiency and superior $SO_2$/$H_2O$ tolerance. The redox property of the catalyst is apparently improved and acidity is greatly enhanced in comparison with Fe/$TiO_2$, due to much intense Fe-O-Ti interaction. *In situ* DRIFTS result indicates there are activated –$NH_2$ and $NO_2$ species on Fe/Ti@Si catalyst, resulting in the activation of reactants and the proceeding of $NH_3$-SCR reaction *via* "fast SCR" route. Importantly, $H_2O$ is found to be conducive for $NH_3$ adsorption on layered titania catalyst, thus an unexpected promotion effect on activity is exhibited. Besides, $SO_2$ is shown to have negligible influence on pre-adsorbed NO and $NH_3$ species, which is responsible for the superior $SO_2$ tolerance. We expect that these results could inspire new insight for designing novel $NH_3$-SCR catalysts with excellent activity and poisoning tolerance for practical applications.

## CRediT authorship contribution statement

**Kai Guo:** Conceptualization, Methodology, Validation, Investigation, Writing - original draft. **Ji Jiawei:** Methodology, Investigation. **Ryota Osuga:** Methodology, Validation, Resources. **Yuxiang Zhu:** Data curation, Formal analysis. **Jingfang Sun:** Validation, Formal analysis. **Changjin Tang:** Writing - review & editing, Data curation, Funding acquisition. **Junko N. Kondo:** Conceptualization, Writing - review & editing, Funding acquisition. **Lin Dong:** Conceptualization, Writing - review & editing, Funding acquisition, Project administration.

## Declaration of Competing Interest

The authors declare that they have no known competing financial interests or personal relationships that could have appeared to influence the work reported in this paper.

## Acknowledgements

The authors gratefully acknowledge the financial support from the National Natural Science Foundation of China (21773106, 21707066, 21806077, 21976081), the Major Scientific and Technological Project of Bingtuan (2018AA002), the Environmental Protection Department of Jiangsu Province (2016048) and the Fundamental Research Funds for the Central Universities (14380236). J. N. Kondo is grateful for the financial support from JST PREST Grant Number JPMJPR1318, Japan. K. Guo greatly appreciates the scholarship support from China Scholarship Council.

## Appendix A. Supplementary data

Supplementary material related to this article can be found, in the online version, at doi:https://doi.org/10.1016/j.apcatb.2021.119982.

## References

[1] J.-A. James, S. Sung, H. Jeong, O.A. Broesicke, S.P. French, D. Li, J.C. Crittenden, Impacts of combined cooling, heating and power systems, and rainwater harvesting on water demand, carbon dioxide, and $NO_x$ emissions for Atlanta, Environ. Sci. Technol. 52 (2018) 3–10.
[2] A. Richter, J.P. Burrows, H. Nüß, C. Granier, U. Niemeier, Increase in tropospheric nitrogen dioxide over China observed from space, Nature 437 (2005) 129–132.
[3] G.C. Borillo, Y.S. Tadano, A.F.L. Godoi, S.S.M. Santana, F.M. Weronka, R. A. Penteado Neto, D. Rempel, C.I. Yamamoto, S. Potgieter-Vermaak, J.H. Potgieter, R.H.M. Godoi, Effectiveness of selective catalytic reduction systems on reducing gaseous emissions from an engine using diesel and biodiesel blends, Environ. Sci. Technol. 49 (2015) 3246–3251.
[4] L. Lietti, I. Nova, G. Ramis, L. Dall'Acqua, G. Busca, E. Giamello, P. Forzatti, F. Bregani, Characterization and reactivity of $V_2O_5$–$MoO_3$/$TiO_2$ De-NOx SCR catalysts, J. Catal. 187 (1999) 419–435.
[5] X. Huang, D. Wang, H. Zhao, Q. Yang, Y. Peng, J. Li, Severe deactivation and artificial enrichment of thallium on commercial SCR catalysts installed in cement kiln, Appl. Catal. B 277 (2020), 119194.
[6] J. Zhang, Z. Huang, Y. Du, X. Wu, H. Shen, G. Jing, Atomic-scale insights into the nature of active sites in $Fe_2O_3$-supported submonolayer $WO_3$ catalysts for selective catalytic reduction of NO with $NH_3$, Chem. Eng. J. 381 (2020), 122668.
[7] H. Wang, Z. Qu, S. Dong, H. Xie, C. Tang, Superior Performance of $Fe_{1-x}W_xO_\delta$ for the Selective Catalytic Reduction of $NO_x$ with $NH_3$: Interaction between Fe and W, Environ. Sci. Technol. 50 (2016) 13511–13519.
[8] M.N. Khan, L. Han, P. Wang, J. He, B. Yang, T. Yan, L. Shi, D. Zhang, $SO_2$-tolerant NOx reduction over ceria-based catalysts: Shielding effects of hollandite Mn-Ti oxides, Chem. Eng. J. 397 (2020), 125535.
[9] Z. Huang, X. Gu, W. Wen, P. Hu, M. Makkee, H. Lin, F. Kapteijn, X. Tang, A "Smart" hollandite DeNOx catalyst: self-protection against alkali poisoning, Angew. Chem. Int. Ed. 52 (2013) 660–664.
[10] Q. Yan, S. Chen, C. Zhang, Q. Wang, B. Louis, Synthesis and catalytic performance of $Cu_1Mn_{0.5}Ti_{0.5}Ox$ mixed oxide as low-temperature $NH_3$-SCR catalyst with enhanced $SO_2$ resistance, Appl. Catal. B 238 (2018) 236–247.
[11] K. Koizumi, H. Yoshida, M. Boero, K. Tamai, S. Hosokawa, T. Tanaka, K. Nobusada, M. Machida, A detailed insight into the catalytic reduction of NO operated by Cr–Cu nanostructures embedded in a $CeO_2$ surface, Phys. Chem. Chem. Phys. 20 (2018) 25592–25601.
[12] C. Tang, H. Zhang, L. Dong, Ceria-based catalysts for low-temperature selective catalytic reduction of NO with $NH_3$, Catal. Sci. Technol. 6 (2016) 1248–1264.
[13] L. Zhang, L. Li, Y. Cao, X. Yao, C. Ge, F. Gao, Y. Deng, C. Tang, L. Dong, Getting insight into the influence of $SO_2$ on $TiO_2$/$CeO_2$ for the selective catalytic reduction of NO by $NH_3$, Appl. Catal. B 165 (2015) 589–598.
[14] H. Liu, Z. Fan, C. Sun, S. Yu, S. Feng, W. Chen, D. Chen, C. Tang, F. Gao, L. Dong, Improved activity and significant $SO_2$ tolerance of samarium modified $CeO_2$-$TiO_2$ catalyst for NO selective catalytic reduction with $NH_3$, Appl. Catal. B 244 (2019) 671–683.
[15] H. Liu, C. Sun, Z. Fan, X. Jia, J. Sun, F. Gao, C. Tang, L. Dong, Doping effect of Sm on the $TiO_2$/CeSmOx catalyst in the $NH_3$-SCR reaction: structure–activity relationship, reaction mechanism and $SO_2$ tolerance, Catal. Sci. Technol. 9 (2019) 3554–3567.
[16] J. Liu, J. Meeprasert, S. Namuangruk, K. Zha, H. Li, L. Huang, P. Maitarad, L. Shi, D. Zhang, Facet–activity relationship of $TiO_2$ in $Fe_2O_3$/$TiO_2$ nanocatalysts for selective catalytic reduction of NO with $NH_3$: in situ DRIFTs and DFT studies, J. Phys. Chem. C 121 (2017) 4970–4979.
[17] S. Yu, Y. Lu, F. Gao, L. Dong, Study on the crystal plane effect of CuO/$TiO_2$ catalysts in $NH_3$-SCR reaction, Catal. Today 339 (2020) 265–273.
[18] Z. Zhang, R. Li, M. Wang, Y. Li, Y. Tong, P. Yang, Y. Zhu, Two steps synthesis of CeTiOx oxides nanotube catalyst: enhanced activity, resistance of $SO_2$ and $H_2O$ for low temperature $NH_3$-SCR of NOx, Appl. Catal. B 282 (2021), 119542.
[19] Y. He, M.E. Ford, M. Zhu, Q. Liu, U. Tumuluri, Z. Wu, I.E. Wachs, Influence of catalyst synthesis method on selective catalytic reduction (SCR) of NO by $NH_3$ with $V_2O_5$-$WO_3$/$TiO_2$ catalysts, Appl. Catal. B 193 (2016) 141–150.
[20] T. Boningari, D.K. Pappas, P.G. Smirniotis, Metal oxide-confined interweaved titania nanotubes M/TNT (M = Mn, Cu, Ce, Fe, V, Cr, and Co) for the selective catalytic reduction of NOx in the presence of excess oxygen, J. Catal. 365 (2018) 320–333.

[21] D.K. Pappas, T. Boningari, P. Boolchand, P.G. Smirniotis, Novel manganese oxide confined interweaved titania nanotubes for the low-temperature Selective Catalytic Reduction (SCR) of NOx by $NH_3$, J. Catal. 334 (2016) 1–13.
[22] S. Yu, N. Jiang, W. Zou, L. Li, C. Tang, L. Dong, A general and inherent strategy to improve the water tolerance of low temperature $NH_3$-SCR catalysts via trace $SiO_2$ deposition, Catal. Commun. 84 (2016) 75–79.
[23] S. Zhan, H. Zhang, Y. Zhang, Q. Shi, Y. Li, X. Li, Efficient $NH_3$-SCR removal of NOx with highly ordered mesoporous $WO_3(\chi)$-$CeO_2$ at low temperatures, Appl. Catal. B 203 (2017) 199–209.
[24] N. Zhang, L. Li, Y. Guo, J. He, R. Wu, L. Song, G. Zhang, J. Zhao, D. Wang, H. He, A $MnO_2$-based catalyst with $H_2O$ resistance for $NH_3$-SCR: study of catalytic activity and reactants-$H_2O$ competitive adsorption, Appl. Catal. B 270 (2020), 118860.
[25] L. Han, S. Cai, M. Gao, J.-y. Hasegawa, P. Wang, J. Zhang, L. Shi, D. Zhang, Selective catalytic reduction of NOx with $NH_3$ by using novel catalysts: state of the art and future prospects, Chem. Rev. 119 (2019) 10916–10976.
[26] D.W. Kwon, K.H. Park, S.C. Hong, Enhancement of SCR activity and $SO_2$ resistance on VOx /$TiO_2$ catalyst by addition of molybdenum, Chem. Eng. J. 284 (2016) 315–324.
[27] C. Liu, L. Chen, J. Li, L. Ma, H. Arandiyan, Y. Du, J. Xu, J. Hao, Enhancement of activity and sulfur resistance of $CeO_2$ supported on $TiO_2$–$SiO_2$ for the selective catalytic reduction of NO by $NH_3$, Environ. Sci. Technol. 46 (2012) 6182–6189.
[28] J. Yu, F. Guo, Y. Wang, J. Zhu, Y. Liu, F. Su, S. Gao, G. Xu, Sulfur poisoning resistant mesoporous Mn-base catalyst for low-temperature SCR of NO with $NH_3$, Appl. Catal. B 95 (2010) 160–168.
[29] K. Guo, G. Fan, D. Gu, S. Yu, K. Ma, A. Liu, W. Tan, J. Wang, X. Du, W. Zou, C. Tang, L. Dong, Pore size expansion accelerates ammonium bisulfate decomposition for improved sulfur resistance in low-temperature $NH_3$-SCR, ACS Appl. Mater. Interfaces 11 (2019) 4900–4907.
[30] D. Zhao, Q. Huo, J. Feng, B.F. Chmelka, G.D. Stucky, Nonionic triblock and star diblock copolymer and oligomeric surfactant syntheses of highly ordered, hydrothermally stable, mesoporous silica structures, J. Am. Chem. Soc. 120 (1998) 6024–6036.
[31] L. Zhurodlev, Colloids Surf, A: phys, Chem. Eng. Aspects 173 (2000) 1–38.
[32] J.N. Kondo, H. Yamazaki, A. Ishikawa, R. Osuga, S. Takao, T. Yokoi, S. Kikkawa, K. Teramura, T. Tanaka, Monolayer tantalum oxide on mesoporous silica substrate, ChemistrySelect 1 (2016) 3124–3131.
[33] J.N. Kondo, Y. Hiyoshi, R. Osuga, A. Ishikawa, Y.-H. Wang, T. Yokoi, Thin (single–triple) niobium oxide layers on mesoporous silica substrate, Microporous Mesoporous Mater. 262 (2018) 191–198.
[34] K. Fukuda, I. Nakai, Y. Ebina, R. Ma, T. Sasaki, Colloidal unilamellar layers of tantalum oxide with open channels, Inorg. Chem. 46 (2007) 4787–4789.
[35] D.A. Svintsitskiy, L.S. Kibis, A.I. Stadnichenko, E.M. Slavinskaya, A.V. Romanenko, E.A. Fedorova, O.A. Stonkus, D.E. Doronkin, V. Marchuk, A. Zimina, M. Casapu, J.-D. Grunwaldt, A.I. Boronin, Insight into the nature of active species of Pt/$Al_2O_3$ catalysts for low temperature $NH_3$ oxidation, ChemCatChem 12 (2020) 867–880.
[36] D. Ye, R. Qu, C. Zheng, K. Cen, X. Gao, Mechanistic investigation of enhanced reactivity of $NH_4HSO_4$ and NO on Nb- and Sb-doped VW/Ti SCR catalysts, Appl. Catal. A 549 (2018) 310–319.
[37] Q. Liang, J. Li, H. He, T. Yue, L. Tong, Effects of $SO_2$ and $H_2O$ on low-temperature NO conversion over F-$V_2O_5$-$WO_3$/$TiO_2$ catalysts, J. Environ. Sci. 90 (2020) 253–261.
[38] F. Liu, W. Shan, Z. Lian, J. Liu, H. He, The smart surface modification of $Fe_2O_3$ by WOx for significantly promoting the selective catalytic reduction of NOx with $NH_3$, Appl. Catal. B 230 (2018) 165–176.
[39] Z. Liu, S. Zhang, J. Li, L. Ma, Promoting effect of $MoO_3$ on the NOx reduction by $NH_3$ over $CeO_2$/$TiO_2$ catalyst studied with in situ DRIFTS, Appl. Catal. B 144 (2014) 90–95.
[40] N. Macleod, R. Cropley, R.M. Lambert, Efficient reduction of NOx by $H_2$ under oxygen-rich conditions over Pd/$TiO_2$ catalysts: an in situ DRIFTS study, Catal. Lett. 86 (2003) 69–75.
[41] J.L. Flores-Moreno, G. Delahay, F. Figueras, B. Coq, DRIFTS study of the nature and reactivity of the surface compounds formed by co-adsorption of NO, $O_2$ and propene on sulfated titania-supported rhodium catalysts, J. Catal. 236 (2005) 292–303.
[42] H. Sjövall, R.J. Blint, L. Olsson, Detailed Kinetic Modeling of $NH_3$ and $H_2O$ Adsorption, and $NH_3$Oxidation over Cu-ZSM-5, J. Phys. Chem. C 113 (2009) 1393–1405.
[43] H. Sjövall, L. Olsson, E. Fridell, R.J. Blint, Selective catalytic reduction of NOx with $NH_3$ over Cu-ZSM-5—the effect of changing the gas composition, Appl. Catal. B 64 (2006) 180–188.
[44] F. Giraud, J. Couble, C. Geantet, N. Guilhaume, S. Loridant, S. Gros, L. Porcheron, M. Kanniche, D. Bianchi, Experimental microkinetic approach of De-NOx by $NH_3$ on $V_2O_5$/$WO_3$/$TiO_2$ catalysts. 6. $NH_3$–$H_2O$ coadsorption on $TiO_2$-Based solids and competitive temkin model, J. Phys. Chem. C 122 (2018) 24634–24651.
[45] J. Shi, Y. Zhang, Z. Zhang, Z. Fan, M. Chen, Z. Zhang, W. Shangguan, Water promotion mechanism on the $NH_3$-SCR over Fe-BEA catalyst, Catal. Commun. 115 (2018) 59–63.
[46] M. Kantcheva, I. Cayirtepe, A. Naydenov, G. Ivanov, FT-IR spectroscopic investigation of the effect of $SO_2$ on the SCR of NOx with propene over $ZrO_2$–$Nb_2O_5$ catalyst, Catal. Today 176 (2011) 437–440.
[47] S. Yang, Y. Guo, H. Chang, L. Ma, Y. Peng, Z. Qu, N. Yan, C. Wang, J. Li, Novel effect of $SO_2$ on the SCR reaction over $CeO_2$: mechanism and significance, Appl. Catal. B 136-137 (2013) 19–28.
[48] L. Wei, S. Cui, H. Guo, X. Ma, L. Zhang, DRIFT and DFT study of cerium addition on $SO_2$ of Manganese-based Catalysts for low temperature SCR, J. Mol. Catal. A 421 (2016) 102–108.
[49] P.A. Kumar, Y.E. Jeong, S. Gautam, H.P. Ha, K.J. Lee, K.H. Chae, XANES and DRIFTS study of sulfated Sb/V/Ce/$TiO_2$ catalysts for $NH_3$-SCR, Chem. Eng. J. 275 (2015) 142–151.
[50] L.J. France, Q. Yang, W. Li, Z. Chen, J. Guang, D. Guo, L. Wang, X. Li, Ceria modified FeMnOx —enhanced performance and sulphur resistance for low-temperature SCR of NOx, Appl. Catal. B 206 (2017) 203–215.